archives
of thermodynamics
Vol. **41**(2020), No. 3, 33–56
DOI: 10.24425/ather.2020.134571

Analysis of thermo-hydraulic performance of a solar air heater tube with modern obstacles

YOUNES MENNI[a]
ALI J. CHAMKHA[*b]
CHAFIKA ZIDANI[a]
BOUMÉDIÈNE BENYOUCEF[a]

[a] Unit of Research on Materials and Renewable Energies, Faculty of Sciences, Abou Bekr Belkaid University of Tlemcen, Algeria

[b] Faculty of Engineering, Kuwait College of Science and Technology, 7th Ring Road, Doha, Kuwait

Abstract This paper presents a numerical analysis on turbulent flow and forced-convection characteristics of rectangular solar air heater tube fitted with staggered, transverse, V-shape, modern obstacles on the heated walls. Air, whose Prandtl number is 0.71, is the working fluid used, and the Reynolds number considered equal to 6×10^3. The governing flow equations are solved using a finite volume approach and the semi-implicit pressure linked equation (SIMPLE) algorithm. With regard to the flow characteristics, the quadratic upstream interpolation for convective kinetics differencing scheme (QUICK) was applied, and a second-order upwind scheme (SOU) was used for the pressure terms. The dynamic thermo-energy behavior of the V-shaped baffles with various flow attack angles, i.e., 50°, 60°, 70°, and 80° are simulated, analyzed, and compared with those of the conventional flat rectangular baffles with attack value of 90°. In all situations, the thermal transfer rate was found to be much larger than unity; its maximum value was around 3.143 for the flow attack angle of 90° and $y = H/2$.

Keywords: Turbulence; Heat transfer; Friction loss; Flow attack; Solar air heater tube

*Corresponding Author. Email: achamkha@pmu.edu.sa

Nomenclature

a	–	thickness of the baffle, m
C_f	–	skin friction coefficient
C_p	–	specific heat at constant pressure, J/kgK
C_μ	–	constant used in the standard k-ε model
D_h	–	hydraulic diameter of the rectangular channel, m
f	–	friction factor
H	–	height of channel, m
h	–	V-baffle height, m
h_x	–	local convective heat transfer coefficient, W/m^{2}K
k	–	turbulent kinetic energy, m^2/s^2
L	–	channel length, m
L_{in}, L_1	–	distance upstream of the first V-baffle, m
L_{out}, L_2	–	distance downstream of the second V-baffle, m
Nu	–	Nusselt number
Nu_x	–	local Nusselt number
$\overline{\mathrm{Nu}}$	–	average Nusselt number
P	–	fluid pressure, Pa
P_{atm}	–	atmospheric pressure, Pa
Pi	–	distance between baffles, m
Pr	–	Prandtl number
Re	–	Reynolds number
T	–	temperature, K
T_{in}	–	inlet temperature, K
T_w	–	wall temperature, K
U_{in}	–	inlet velocity, m/s
$\overline{U}$	–	channel average velocity, m/s
W	–	width of channel, m
u	–	fluid velocity in the x-direction, m/s
v	–	fluid velocity in the y-direction, m/s
x, y	–	Cartesian coordinates, m

Greek symbols

θ	–	angles of flow attack, $^\circ$
λ	–	thermal conductivity, W/m K
μ	–	dynamic viscosity, kg/m s
μt	–	eddy viscosity, kg/m s
ν	–	kinematics viscosity, kg/m s
ρ	–	fluid density, kg/m^3
σ_k	–	constant used in the standard k-ε model
σ_ε	–	constant used in the standard k-ε model
τ_w	–	wall shear stress, Pa
ω	–	turbulent dissipation rate, m^2/s^3

Subscripts

atm	–	atmospheric
f	–	fluid
in	–	inlet of the computational domain
s	–	solid
t	–	turbulent
w	–	wall

1 Introduction

The first study on the numerical analysis of the features of the flow and forced-convection heat transfer in a channel was reported by Patankar *et al.* [1]. The authors exposed the concepts of periodically fully-developed flow and heat transfer. Bergeles and Athanassiadis presented measurements of the length of the recirculating region behind the obstacle as a function of the obstacle width and some velocities at one location outside the region of recirculation [2]. The obtained results showed that upstream of the obstacle, the length of the main recirculating region remains unchanged with obstacle width and equal to $0.85H$; however the downstream length of the recirculating region is a strong function of the width and changes almost linearly from 11 obstacle heights for $W/H = 1.0$ to 3 for W/H greater than four. Nemec *et al.* [3] experimentally revealed that the most influential factors on performance of the heat pipe are mainly geometric parameters of capillary structures and thermophysical properties of the working fluid. The effect of these factors on the dynamics of heat transfer by heat pipes can be easily identified by thermovision scanning surface temperatures of heat pipes.

Prasad and Saini enhanced the convective heat transfer coefficient between absorber plate and air in a flat-plate solar air heater by providing the absorber plate with artificial roughness [4]. The effect of height and pitch of the roughness elements on the heat transfer rate and friction was investigated.

Yeh and Chou carried out experimental studies to investigate the improvement in the collector efficiency of solar air heaters under the influence of baffles attached to the fins [5]. Considerable improvement in the collector efficiency of solar air heaters is obtained if the fins in the collector are provided with attached baffles to create air turbulence and extended heat-transfer area.

Bartoszewicz and Bogusławski reported the results of numerical simulations of the steam flow in a shell and tube heat exchanger [6]. They tested the efficiency of different models of turbulence. The results of numerical studies were verified experimentally for a real heat exchanger. Modification of the inlet flow direction according to theoretical considerations caused the increase of thermal power of a heat exchanger of about 14%. Acharya *et al.* [7] conducted a numerical investigation to obtain detailed laser-Doppler measurements of the flow in the upstream and downstream recirculation regions of a separated duct flow past a wall-mounted, two-dimensional rib and to evaluate the ability of the nonlinear k-ε model to predict the flow behavior. The measurements demonstrated that the turbulence was far from equilibrium in the recirculation and shear layer regions, with non-equilibrium conditions persisting at least as far as 7 rib heights downstream of reattachment.

Yeh *et al.* [8] made studies to investigate theoretically the effect of aspect ratio on the collector efficiency of baffled solar air heaters for constant collector area and constant flow rate. With constant collector area, the collector efficiency increases when the collector aspect ratio increases.

Muszyński and Koziełcarried out two-dimensional numerical investigations of the fluid flow and heat transfer for the laminar flow of the louvered fin-plate heat exchanger, designed to work as an air-source heat pump evaporator [9]. The simulations were performed for different geometries with varying louver pitch, louver angle and different louver blade number. The maximum heat transfer improvement interpreted in terms of the maximum efficiency was obtained for the louver angle of 16° and the louver pitch of 1.35 mm.

Sara *et al.* [10] investigated experimentally the enhancement of the convective heat transfer from a flat surface due to rectangular cross-sectional blocks in a parallel flow in a rectangular duct. The authors aimed to analyze the thermal performances of these heat transfer promoters with respect to their heat transfer enhancement efficiencies for a constant pumping power.

Murata and Mochizuki numerically simulated the heat transfer in a rib-roughened duct by using the second-order finite difference method in coordinates fitted to transverse or angled ribs [11]. Turbulent and laminar cases of which Reynolds numbers were 350 and 50, respectively, were computed for rib angles of 60° and 90°. The comparison between the laminar and turbulent results showed clear differences in heat transfer distribution because the higher momentum fluid of the turbulent case was more disturbed by the ribs as compared to the laminar case.

Cieśliński *et al.* [12] conducted an investigation of selected type of brazed plate heat exchanger (PHEx), to experimentally check ability of several correlations published in the literature to predict heat transfer coefficients by comparison experimentally obtained data with appropriate predictions. They obtained revealed that Hausen and Dittus–Boelter correlations underestimated heat transfer coefficient for the tested PHEx by an order of magnitude.

Demartini *et al.* [13] analyzed the turbulent flow of air through a rectangular channel containing two baffle plates. A comprehensive analysis of the velocity profiles and pressure gradients was carried out in this work. Hot wire anemometry and the finite volume method, by means of commercial program Fluent, were applied in this research work. Dutta and Hossain experimentally investigated the local heat transfer characteristics and the associated frictional head loss in a rectangular channel with inclined solid and perforated baffles [14]. A combination of two baffles of same overall size was used in this experiment. The upstream baffle was attached to the top heated surface, while the position, orientation, and the shape of the other baffle were varied to identify the optimum configuration for enhanced heat transfer.

Duda and Mazurkiewicz reported a numerical modeling of steady state heat and mass transfer in cylindrical ducts [15]. Both laminar and hydrodynamically fully developed turbulent flows were shown. Numerical results were compared with values obtained from analytical solution of such problems. They occurred in heat exchangers using liquid metals as working fluid, in cooling systems for electric components or in chemical process lines. Calculations were carried out gradually decreasing the mesh size in order to examine the convergence of numerical method to analytical solution. Tandiroglu experimentally studied the effect of the flow geometry parameters on transient forced convection heat transfer for turbulent flow in a circular tube with baffle inserts [16]. Different geometrical parameters such as the baffle spacing, and the baffle orientation angle were varied. A numerical study of the forced convection heat transfer in a smooth circular tube was conducted by Nasiruddin and Kamran Siddiqui [17]. A baffle was introduced in the domain to produce a vortex to enhance mixing and thus, the heat transfer. The effects of baffle size and orientation on the heat transfer enhancement were studied in detail. Three different baffle arrangements were considered. Zima and Dziewa presented a one-dimensional mathematical model for simulating the transient processes which occur in the liquid flat-plate solar collector tubes [18]. The proposed method con-

sidered the model of collector tube as one with distributed parameters. In the suggested method one tube of the collector was taken into consideration. In this model the boundary conditions can be time-dependent. Two numerical analyses were performed: for the tube with temperature step function of the fluid at the inlet and for the tube with heat flux step function on the outer surface. In both cases the conformity of results was very good.

Kahalerras and Targui numerically studied the heat transfer enhancement in a double pipe heat exchanger by using porous fins attached at the external wall of the inner cylinder [19]. The effects of several geometrical, physical and thermal parameters such as fins spacing and height, Darcy number and the thermal conductivity ratio on the structure of the hydrodynamic and thermal fields were analyzed.

Sripattanapipat and Promvonge numerically investigated the laminar periodic flow and heat transfer in a two dimensional horizontal channel with isothermal walls and with staggered diamond-shaped baffles [20]. Effects of different baffle tip angles on heat transfer and pressure loss in the channel were studied and the results of the diamond baffle were also compared with those of the flat baffle.

Rao *et al.* [21] conducted an experimental and numerical study to investigate the flow friction and heat transfer performance in rectangular channels with staggered arrays of pin fin-dimple hybrid structures and pin fins in the Reynolds number range of 8 200–54 000. The study aimed at improving the cooling design for the gas turbine components. The friction factor, Nusselt number and the overall thermal performance parameters of the pin fin-dimple and the pin fin channels were obtained and compared with the experimental data of a smooth rectangular channel and previously published data of the pin fin channel.

Alam *et al.* [22] experimentally investigated the effect of geometrical parameters of the V-shaped perforated blocks on heat transfer and flow characteristics of rectangular duct. Thermal-hydraulic performance of V-shaped perforated blockages was also compared to that of V-shaped solid blockages for same geometrical parameters. Kumar and Kim [23] reviewed the investigations carried out by various investigators to enhance heat transfer and pressure drop by the use of ribs and baffles of different shapes, sizes, and orientations to produce artificial roughness. In this work a comparative study were also carried out to select best rib and baffle roughness shapes for maximum heat transfer rate and minimum pressure drop losses. Kumar *et al.* [24] presented an experimental study on heat transfer and

friction characteristics of solar air channel fitted with discretized broken V-pattern baffle on the heated plate. The effect of geometrical parameters, predominantly the gap width and gap location was investigated. The optimal values of geometrical parameters of roughness were obtained and discussed.

Numerical and experimental works for both simple and modern obstacles in channels for the turbulent flow (Wang *et al.* [25]; Chamoli [26]; Du *et al.* [27]) and for the laminar flow regimes (Mohammadi Pirouz *et al.* [28]; Jedsadaratanachai *et al.* [29]; Zhao *et al.* [30]) were conducted and heat transfer and friction performance results for both the simple and modern cases were reported. Other similar numerical and experimental studies can be found in the literature as Tahmasebi *et al.* [31], Mehryan *et al.* [32–34], Ghalambaz *et al.* [35–37], and Chamkha *et al.* [38]. In those studies, different structural parameters and various obstacle geometries were employed.

This study conducted computational fluid dynamical (CFD) simulation and established mathematical model to discuss the dynamic thermo-energy performance of the novel air collector. In this contribution, a thermo-hydrodynamic analysis for turbulent airflow in a rectangular solar air heater tube fitted with V-shape, modern-type obstacles mounted on both top and bottom walls are conducted in order to investigate the deformation in the fluid flow field and thermal transfer rate performance. Air was used as a working fluid.

2 Computational domain

2.1 Flow geometry

Computational domain for the present problem is shown in Fig. 1. It is a two-dimensional, horizontal, of rectangular cross section, solar air heater tube incorporating two transverse, V-shape, solid-type obstacles pointing upstream with different angles of flow attack (θ) of 50°, 60°, 70°, and 80°, and mounted on both top and bottom hot surfaces in a staggered manner as shown in Fig. 1(a). Also, a simple flat rectangular obstacle with an angle of attack of 90°, without changing the structural parameters a (V-section thickness) and h (V-section height) is inserted for validation and comparison.

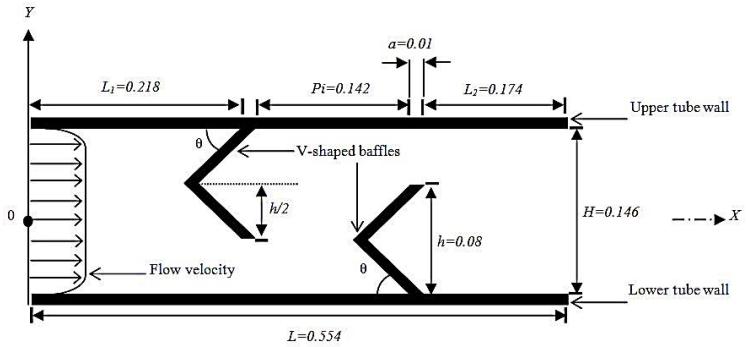

(a)

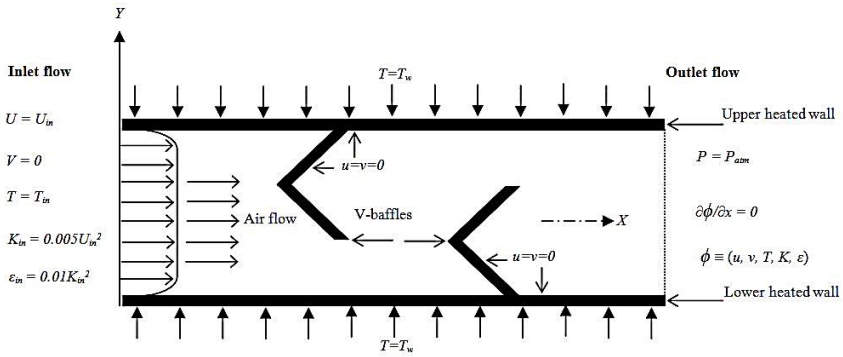

(b)

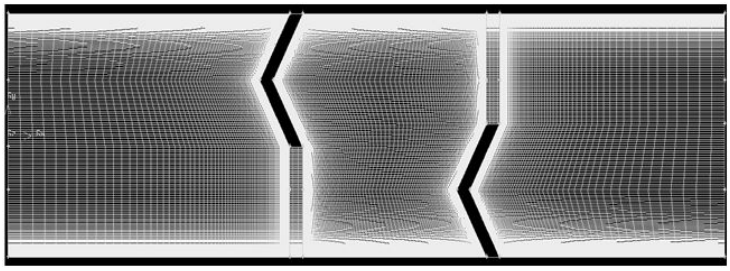

(c)

Figure 1: Problem under examination: (a) two-dimensional rectangular solar air heater tube (dimension in m), (b) thermal-hydrodynamic boundary conditions, and (c) mesh [39].

2.2 Physical model

The physical model for flow and thermal transfer in the given computational domain is developed under the following assumptions: (i) steady

two-dimensional fluid flow and heat transfer; (ii) flow is turbulent and incompressible; (iii) constant fluid properties; and (iv) body forces, viscous dissipation, and radiation heat transfer are ignored.

2.3 Governing equations

Based on the above assumptions, the tube flow is governed by the continuity equation, the Navier–Stokes equations and the energy equation. In the Cartesian tensor system $(i, j = 1, 2, 3)$ these equations can be written as follows [40]:

continuity equation

$$\frac{\partial}{\partial x_i}\left(\rho u_i\right) = 0\,, \tag{1}$$

momentum equation

$$\rho u_j \frac{\partial u_i}{\partial x_j} = \frac{\partial}{\partial x_j}\left[\left(\mu + \mu_t\right)\frac{\partial u_i}{\partial x_j}\right] - \frac{\partial P}{\partial x_i}\,, \tag{2}$$

energy equation

$$\rho u_j \frac{\partial T}{\partial x_j} = \frac{\partial}{\partial x_j}\left[\left(\frac{\mu}{\mathrm{Pr}} + \frac{\mu_t}{\mathrm{Pr}_t}\right)\frac{\partial T}{\partial x_j}\right]\,. \tag{3}$$

2.4 Shear-stress transport k-ω model

The shear-stress transport (SST) k-ω turbulent model is defined by two transport equations, one for the turbulent kinetic energy (k), and the other for the specific dissipation rate (ω), as given below [17]:

$$\frac{\partial}{\partial x_i}\left(\rho\, k\, u_i\right) = \frac{\partial}{\partial x_j}\left(\Gamma_k \frac{\partial k}{\partial x_j}\right) + G_k - Y_k + S_k\,, \tag{4}$$

$$\frac{\partial}{\partial x_i}\left(\rho\, \omega\, u_i\right) = \frac{\partial}{\partial x_j}\left(\Gamma_\omega \frac{\partial \omega}{\partial x_j}\right) + G_\omega - Y_\omega + D_\omega + S_\omega\,. \tag{5}$$

In Eqs. (4) and (5), G_k represents the generation of turbulence kinetic energy due to mean velocity gradients, G_ω represents the generation of ω, Γ_k and Γ_ω represent the effective diffusivity of k and ω, respectively, Y_k and Y_ω represent the dissipation of k and ω due to turbulence, D_ω represents the cross-diffusion term, S_k and S_ω are user-defined source terms.

2.5 Boundary conditions

Thermal and hydrodynamic boundaries are summarized as follows: (i) in the inlet region, a uniform one-dimensional velocity profile was prescribed [13, 17], as shown in Fig. 1b; (ii) impermeable boundary and no-slip wall conditions were applied to all the solid walls; (iii) constant temperature (T_w) of 375 K was applied on the entire walls of the tube as the thermal boundary condition [17]; (iv) temperature of the working fluid (T_{in}) was set equal to 300 K at the inlet of the tube [17]; and (v) in the tube outlet it is prescribed the atmospheric pressure (P_{atm}) [13].

2.6 Governing parameters

The flow Reynolds number (Re) based on the channel hydraulic diameter

$$D_h = 2HW/(H+W) \tag{6}$$

is given by

$$\mathrm{Re} = \frac{\rho U_{in} D_h}{\mu}. \tag{7}$$

The dynamic pressure coefficient can be obtained by

$$C_p = \frac{P - P_{atm}}{(\rho U_{in}^2)/2}. \tag{8}$$

The skin friction coefficient is given by

$$C_f = \frac{\tau_w}{(\rho U_{in}^2)/2}. \tag{9}$$

The friction factor is evaluated from the pressure drop (ΔP) as

$$f = \frac{(\Delta P/D_h)}{(\rho U_{in}^2)/2}. \tag{10}$$

The local Nusselt number can be written as

$$\mathrm{Nu}_x = \frac{h_x D_h}{k_f} \tag{11}$$

and the average Nusselt number can be obtained by

$$\mathrm{Nu} = \frac{1}{L}\int \mathrm{Nu}_x \dot{\mathrm{x}}, \tag{12}$$

where L, H, and W are the channel length, height and width, respectively, U_{in} represents the inlet velocity, τ_w is the shear stress to the wall, μ is the fluid dynamic viscosity, ρ is the fluid density; P is the static pressure; and P_{atm} is the atmospheric pressure.

The Dittus and Boelter correlation has the form [41]

$$\mathrm{Nu}_0 = 0.023\,\mathrm{Re}^{0.8}\,\mathrm{Pr}^{0.4} \quad \text{for} \quad \mathrm{Re} \geq 10^4\,. \tag{13}$$

The Petukhov correlation has the form [42]:

$$f_0 = (0.79\ln \mathrm{Re} - 1.64)^{-2} \quad \text{for} \quad 3\times 10^3 \leq \mathrm{Re} \leq 5\times 10^6. \tag{14}$$

The quantities Nu_0 and f_0 are the average Nusselt number and friction factor of the smooth channel, respectively.

3 Method and procedure

The governing equations employed to simulate the fluid flow and heat transfer in the whole domain investigated were integrated through the finite volume method (FVM using a two-dimensional formulation with the semi-implicit pressure linked equation (SIMPLE) algorithm for pressure velocity coupling), details of which can be found in Patankar [43]. With regard to the flow characteristics, the quadratic upstream interpolation for convective kinetics differencing (QUICK) scheme was applied [44], and the second-order upwind (SOU) scheme was used for pressure terms [43]. The two-dimensional mesh is structured with quadrilateral-type elements, Fig. 1(c). The grid system of (190×85) nodes, in x- and y-directions, respectively, with finer resolution near the all solid boundaries was adopted for the model under consideration.

4 Results and discussion

The numerical runs are carried out for different values of Reynolds numbers (Re = 12 000, 17 000, 22 000, 27 000, and 32 000) at constant wall temperature condition along the top and bottom walls. The simulation results are then analyzed to explain the hydrodynamic and heat transfer phenomena occurring in the system. For the presentation of the contour plots of thermo-hydrodynamic fields, Re = 12 000 is chosen as the base case.

The purpose of present computational analysis is to examine the dynamic thermal-energy behavior of air inside a rectangular cross section,

solar air heater tube, containing two transverse, staggered, solid-type, V-shape baffles as presented numerically and experimentally in more detail in Demartini *et al.* [13]. In that study, the airflow through a two-dimensional horizontal channel, where two flat rectangular baffle plates were placed in opposite channel surfaces, was treated.

The structural parameters of the simple baffled channel are [13]: length of the channel $L = 0.554$ m; height of the channel $H = 0.146$ m; width of the channel $W = 0.193$ m; thickness of the baffle $a = 0.01$ m; distance between baffles $Pi = 0.142$ m; distance between the channel inlet and the first baffle $L_1 = 0.218$ m; distance between the second baffle and the channel exit $L_2 = 0.174$ m; distance between the upper edge of the baffle and the opposite wall was kept constant at $h = 0.08$ m. The channel hydraulic diameter $D_h = 0.167$ m, and velocity of air particles at the inlet $U_{in} = 7.8$ m/s (for $\mathrm{Re} = 8.73 \times 10^4$).

4.1 Numerical validation

To verify the CFD simulation, a comparison of dynamic pressure coefficient (C_p) between the present computational analysis and the numerical and experimental results [13] is shown in Fig. 2 for $\mathrm{Re} = 8.73 \times 10^4$. The plot

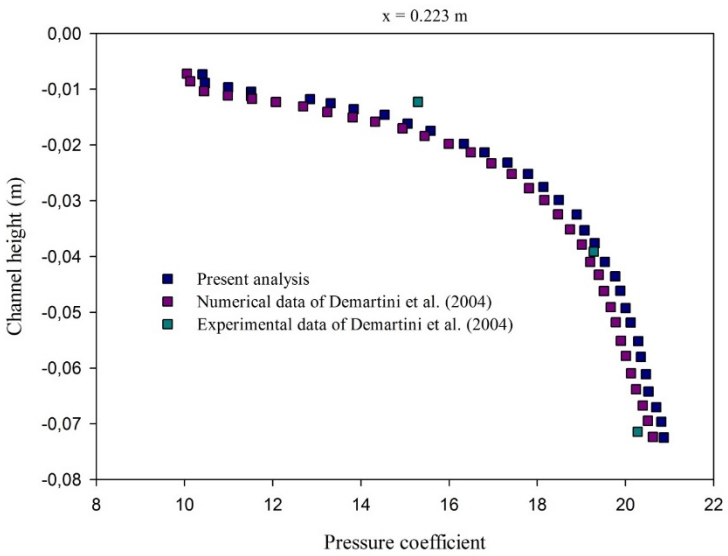

Figure 2: Validation of present dynamic pressure coefficient (C_p) results with experimental and numerical data [13], $\mathrm{Re} = 8.73 \times 10^4$.

in Fig. 2 shows the distribution of the dynamic pressure coefficient profiles in the line starting from the tip of the first baffle plate to the opposite wall, at $x = 0.223$ m from the entrance. It is clear from this figure that the comparison results show a good agreement.

4.2 Fluid flow analysis

4.2.1 Streamlines

Figure 3 (a) to (e) shows the contour plots of streamlines for the case of different attack angles at $\mathrm{Re} = 6 \times 10^3$. The plots reveal the existence of three main regions. In the first area, just upstream of the wall-mounted V-shaped baffles, the fluid is accelerated and arrives with the axial speed. At the approach of the upper and lower wall-attached obstacles, the current lines are deflected. In the second region, located between the top of each obstacle and the walls of the tube, the flow is accelerated due to the effect of cross-sectional reduction. In the third region, downstream of the obstacles, the current lines are generated by the effect of flow expansion, thus leaving the section formed by the V-obstacles and the walls. The most important phenomenon occurring in this zone is the formation of a recirculating flow whose extent is proportional to the flow attack angle (θ).

4.2.2 Mean velocity

Figure 4 (a) to (e) shows the computational results of mean velocity distributions in the whole domain examined when $\mathrm{Re} = 6 \times 10^3$. It can clearly be noticed that the values of the fluid velocity are very low in the vicinity of the two V-obstacles, especially in the downstream regions; this is due to the presence of the recirculation zones. Far from these zones, the current lines become parallel, which results in the progressive development of the flow. One should also note that the velocity increases in the space between the end of each obstacle and the wall of the tube. This rise in velocity is generated first by the presence of the obstacles and then by the presence of recirculation which results in a sudden change in the direction of the flow. It is also observed that the highest values of the velocity appear near the top of the tube, with an acceleration process that begins just after the second obstacle, thus approaching values of the order of 443.807% of the inlet velocity. From the figure, it can clearly be seen that the velocity is proportional to the flow attack angle, for the case of the configuration under study.

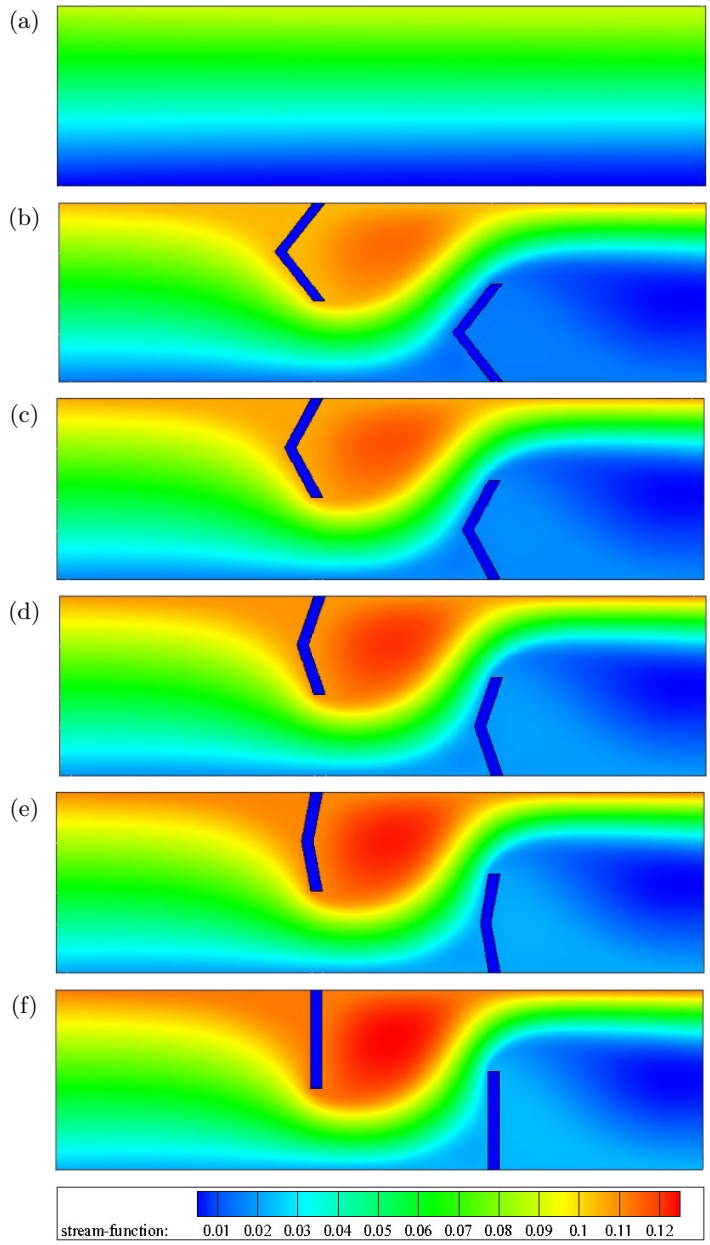

Figure 3: Contours of stream function for various cases for various flow attack angles at $\mathrm{Re} = 6 \times 10^3$: (a) smooth rectangular tube with no baffle, (b) tube with 50° V-baffles, (c) tube with 60° V-baffles, (d) tube with 70° V-baffles, (e) tube with 80° V-baffles, and (f) tube with flat rectangular baffles ($\theta = 90°$). Flow is from left to right. Stream function values in kg/s.

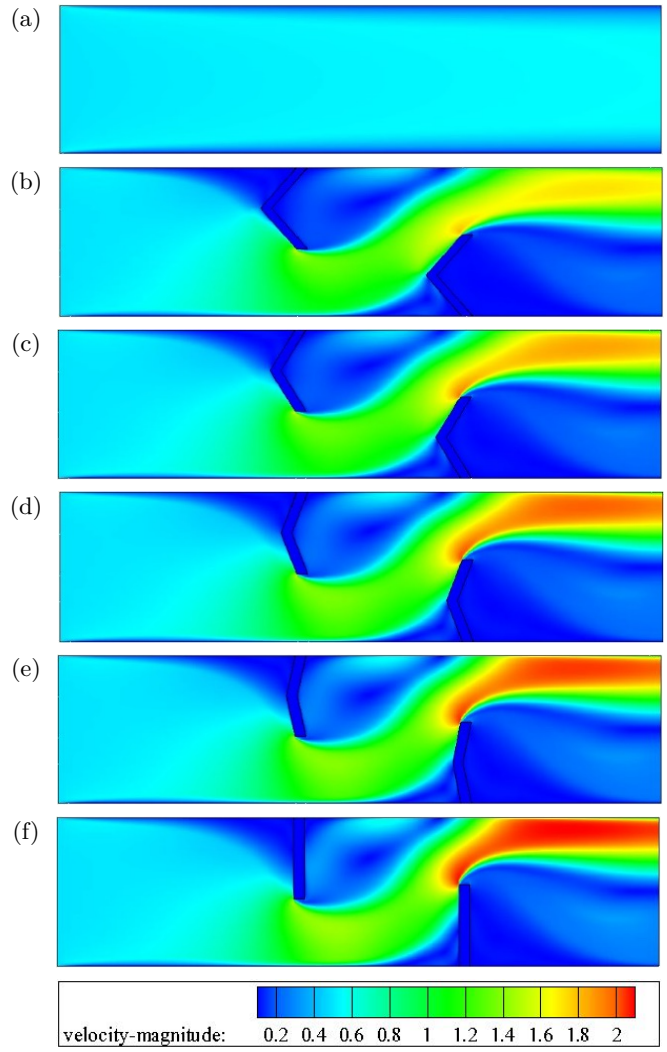

Figure 4: Contours of velocity magnitude for various cases at $\mathrm{Re} = 6 \times 10^3$: (a) smooth rectangular tube with no baffle, (b) tube with 50° V-baffles, (c) tube with 60° V-baffles, (d) tube with 70° V-baffles, (e) tube with 80° V-baffles, and (f) tube with flat rectangular baffles ($\theta = 90°$). Flow is from left to right. Mean velocity values in m/s.

4.2.3 Axial velocity

Figure 5 (a) to (b) shows the velocity field for the same Reynolds number, $\mathrm{Re} = 6 \times 10^3$. As illustrated in this figure and similar to the results in

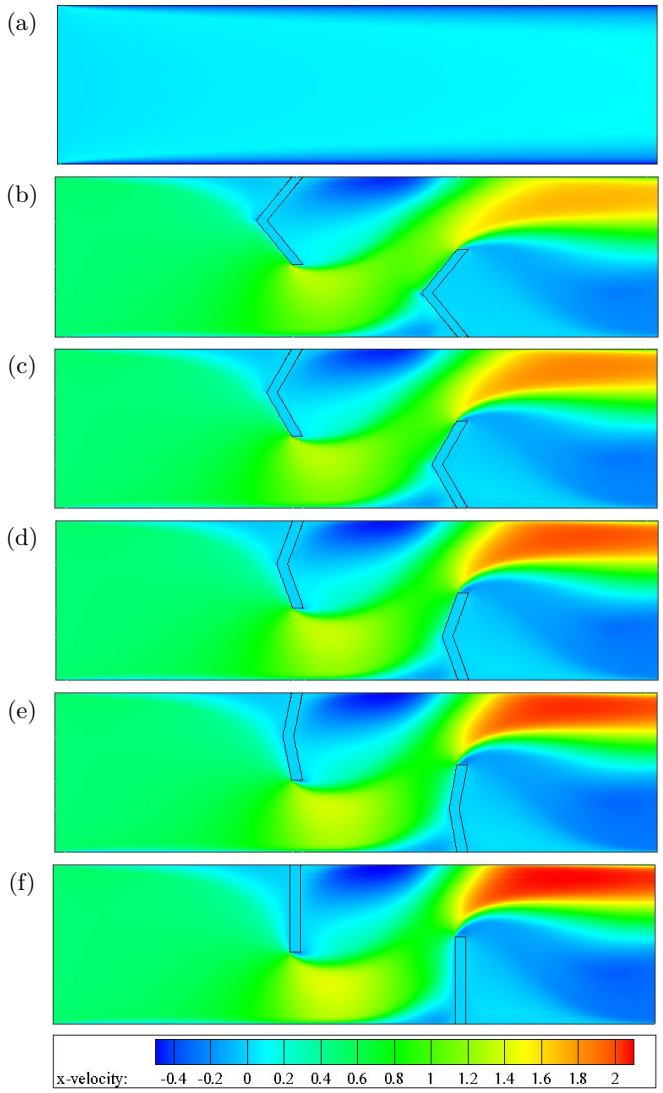

Figure 5: Contours of axial velocity for various cases $\mathrm{Re} = 6\times10^3$: (a) smooth rectangular tube with no baffle, (b) tube with 50° V-baffles, (c) tube with 60° V-baffles, (d) tube with 70° V-baffles, (e) tube with 80° V-baffles, and (f) tube with flat rectangular baffles ($\theta = 90°$). Flow is from left to right. Axial velocity values in m/s.

Fig. 4 (a) to (e) of the mean velocity fields, the axial velocity values are very low next to the obstacles, especially in the back areas, because of the existence of recirculation cells. In areas confined between the upper sides

of the obstacles and the inner walls of the tube, the axial velocity values increase. The values of axial velocity are maximal next to the upper surface of the airway near the exit, also near the top left side of the lower wall-mounted baffle, due to the high speed of air flow in these regions. What was also observed, there is a direct correlation between the increase in the flow attack angle and the rise in values of the flow axial velocity. In addition, the flat baffled tube flows give higher values of velocity than that for V-shaped baffled tube or smooth tube flow in all cases.

4.2.4 Turbulent kinetic energy

The effect of changing flow attack angle values on the flow structure in terms of turbulent kinetic energy (TKE) for the tube with simple (flat, rectangular shape) and modern (V-shape) obstacles is represented in Fig. 6 (a) to (e). The values of TKE range from negligible at small attack angle values in different areas of the tube, to weak at intermediate attack angle values from the upper wall-mounted fin through the lower wall-mounted V-fin to the exit, to considerable at the large values of flow attack angle. We record the marginal values of TKE on the sides of the top free upper wall-mounted baffle face and the lower wall-mounted baffle tip. An increase in attack angle values increases TKE values by forming a severer loop in the free input above the second baffle near the heated top wall of the tube. In these marginal areas, the solid surfaces of the tube and the obstacles exhibit the greatest resistance to fluid movement as a result of strong change in the flow path at high values of velocity and pressure due to the decrease in the cross-section, which is estimated at 54.794% in this study case.

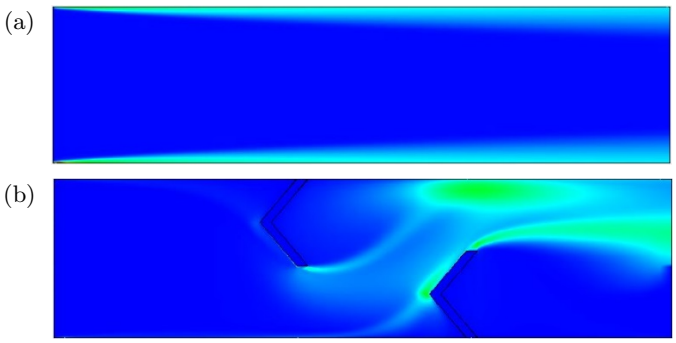

Figure 6: (a) and (b).

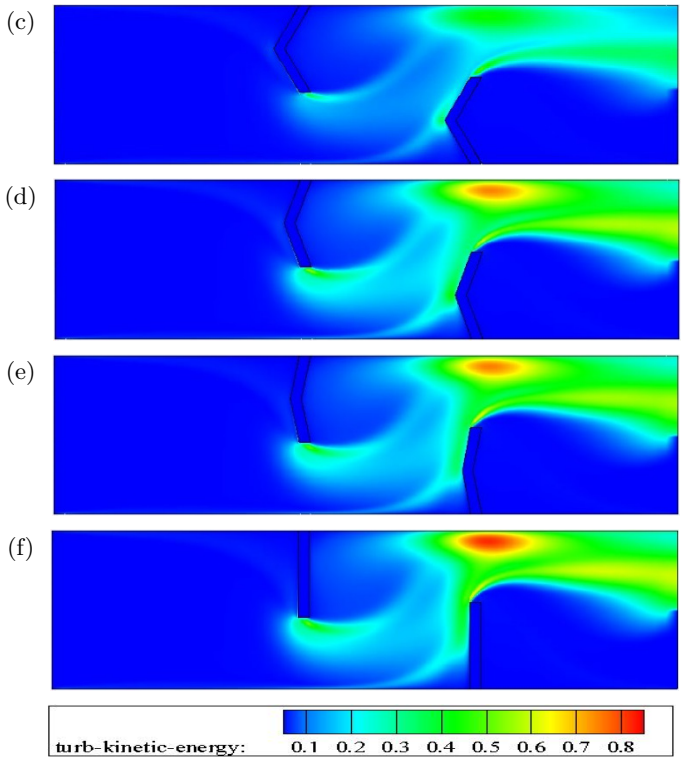

Figure 6: Contours of turbulent kinetic energy for various cases $\mathrm{Re} = 6 \times 10^3$: (a) smooth rectangular tube with no baffle, (b) tube with 50° V-baffles, (c) tube with 60° V-baffles, (d) tube with 70° V-baffles, (e) tube with 80° V-baffles, and (f) tube with flat rectangular baffles ($\theta = 90°$). Flow is from left to right. Turbulent kinetic energy values in $\mathrm{m}^2/\mathrm{s}^2$.

4.3 Heat transfer analysis

4.3.1 Isotherms

The isotherm contours obtained for different values of attack angle are shown in Fig. 7 (a) to (e). This flow structure has a considerable influence on the distribution of the temperature field; it allows a better mixing of the fluid which stimulates the transfer of heat, as will be seen hereafter (Fig. 8). The temperature field shown indicates a temperature drop in the regions situated between the end of each obstacle and the walls of the tube, with an acceleration process that begins just after the first obstacle. Moreover, the temperature field shows that the air temperature in the recycling zone,

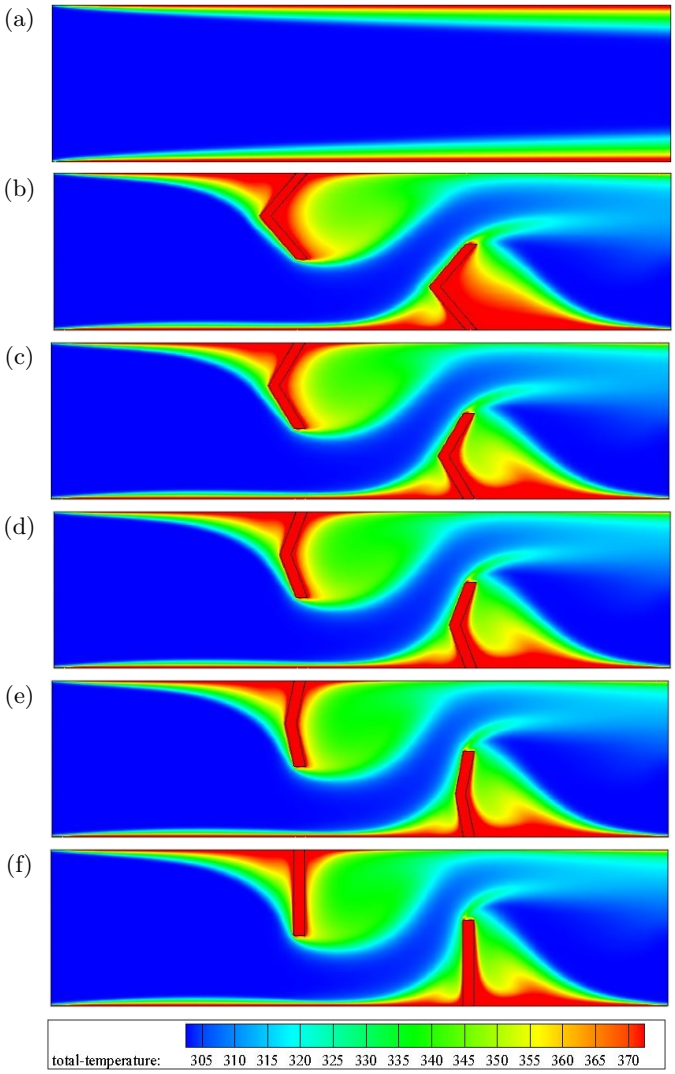

Figure 7: Contours of temperature for various cases $\mathrm{Re} = 6 \times 10^3$: (a) smooth rectangular tube with no baffle, (b) tube with 50° V-baffles, (c) tube with 60° V-baffles, (d) tube with 70° V-baffles, (e) tube with 80° V-baffles, and (f) tube with flat rectangular baffles ($\theta = 90°$). Flow is from left to right. Temperature values in K.

downstream of the obstacle, is slightly higher than that obtained in the same region, but without any fins. In the region around the second obstacle, recycling cells are observed but with a quite low temperature.

4.3.2 Nusselt number

We conducted an average study on the normalized Nusselt number ($\mathrm{Nu}/\mathrm{Nu}_0$) distribution along the upper wall of the tube, as shown in Fig. 8. The upper wall-mounted obstacle directs the flow towards the bottom wall, but the lower wall-mounted obstacle guides it towards the upper wall, and this allows the fluid to capture all the thermal energy from the hot wall. In the figure, the normalized average Nusselt numbers, are related as a function of attack angle ($\theta = 50°$, $60°$, $70°$, $80°$, and $90°$) at the surface of the upper tube wall for a constant value of the Reynolds number, $\mathrm{Re} = 6 \times 10^3$. In the plot, it is interesting to note that the heat transfer rate tends to augment with the augmentation in the flow attack angles for the same Reynolds number applied. For the range examined, the simple or modern baffled tube flows give upper rates of heat transfer than that for smooth tube flow with no obstacle due to the introduction of large recirculation cells in the channel with baffles and fins, leading to upper temperature gradients. The top value of attack of flow leads to an augmentation in heat transfer rates. However, it can be noted that for all situations under study, the case of flat rectangular baffled tube ($\theta = 90°$) shows better heat transfer rate distributions.

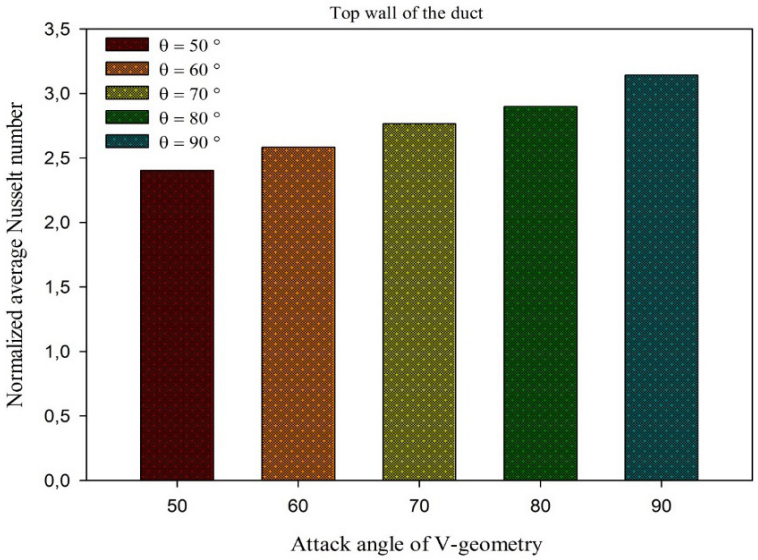

Figure 8: Normalized average Nusselt number ($\mathrm{Nu}/\mathrm{Nu}_0$) for various cases, $\mathrm{Re} = 6 \times 10^3$.

4.4 Skin friction analysis

The effect of the change in attack angle on the diagram of the normalized friction factor, along the upper wall, is shown in Fig. 9. When the angle of flow attack rises from 50° to 90°, the normalized factor of friction increases significantly, thus introducing large recirculation zones (see Fig. 3). This observation is also confirmed by the evolution of the mean and axial velocities, as shown in Figs. 4 and 5, respectively. The angle of attack has an impact on the average coefficient of normalized friction (f/f_0); a correlation exists between the two variables. Indeed, increasing the attack angle results in a substantial growth in the fluid velocity; the losses due to skin friction are also very significant.

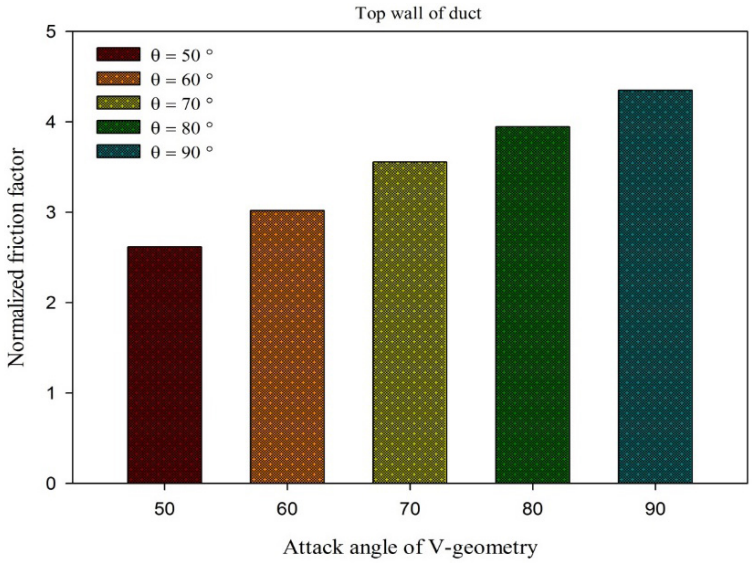

Figure 9: Normalized friction factor (f/f_0) for various cases, Re $= 6 \times 10^3$.

5 Conclusions

Among the parameters that have an impact on the flow structure and heat transfer, the angle of attack of flow is of particular interest in this study. The governing flow equations were solved using the finite volume method based on the SIMPLE discretization algorithm. The shear stress transport k-ω model was used to model turbulence. The dynamic thermo-energy be-

havior was presented in terms of stream function, velocity magnitude, axial velocity, turbulent kinetic energy, temperature, normalized Nusselt number, and friction loss. The pressure loss in terms of normalized friction factor of 50°−80° V-shaped obstacles (the different flow attack angles) was lower than that of simple flat rectangular obstacles (flow attack angle of 90°), which indicates that the obstacle of V-form is more advantageous than the others, at the same value of the Reynolds number.

Received 14 January 2019

References

[1] Patankar S.V., Liu C.H., Sparrow E.M.: *Fully developed flow and heat transfer in ducts having streamwise-periodic variations of cross-sectional area.* J. Heat Trans-T ASME **99** (1977), 2, 180–186.

[2] Bergeles G., Athanassiadis N.: *The flow past a surface-mounted obstacle.* J. Fluid. Eng. **105** (1983), 4, 461–463.

[3] Nemec P., Čaja A., Lenhard R.: *Visualization of heat transport in heat pipes using thermocamera.* Arch. Thermodyn. **31** (2010), 4, 125–132.

[4] Prasad B.N., Saini J.S.: *Effect of artificial roughness on heat transfer and friction factor in a solar air heater.* Sol. Energy **41** (1988), 6, 555–560.

[5] Yeh H.M., Chou W.H.: *Efficiency of solar air heaters with baffles.* Energy **16** (1991), 7, 983–987.

[6] Bartoszewicz J., Bogusławski L.: *Numerical analysis of the steam flow field in shell and tube heat exchanger.* Arch. Thermodyn. **37** (2016), 2, 107–120.

[7] Acharya S., Dutta S., Myrum T.A., Baker R.S.: *Turbulent flow past a surface-mounted two-dimensional rib.* J. Fluid. Eng. **116** (1994), 2, 238–246.

[8] Yeh H.M., Ho C.D., Lin C.Y.: *The influence of collector aspect ratio on the collector efficiency of baffled solar air heaters.* Energy **23** (1998), 1, 11–16.

[9] Muszyński T., Kozieł S.M.: *Parametric study of fluid flow and heat transfer over louvered fins of air heat pump evaporator.* Arch. Thermodyn. **37**(2016), 3, 45–62.

[10] Şara O.N., Pekdemir T., Yapici S., Erşahan H.: *Thermal performance analysis for solid and perforated blocks attached on a flat surface in duct flow.* Energ. Convers. Manage. **41**(2000), 10, 1019–1028.

[11] Murata A., Mochizuki S.: *Comparison between laminar and turbulent heat transfer in a stationary square duct with transverse or angled rib turbulators.* Int. J. Heat Mass Tran. **44**(2001), 6, 1127–1141.

[12] Cieśliński J.T., Fiuk A., Typiński K., Siemieńczuk B.: *Heat transfer in plate heat exchanger channels: Experimental validation of selected correlation equations.* Arch. Thermodyn. **37**(2016), 3, 19–29.

[13] Demartini L.C., Vielmo H.A., Möller S.V.: *Numeric and experimental analysis of the turbulent flow through a channel with baffle plates.* J. Braz. Soc. Mech. Sci. Eng. **26**(2004), 2, 153–159.

[14] Dutta P., Hossain A.: *Internal cooling augmentation in rectangular channel using two inclined baffles*. Int. J. Heat Fluid Fl. **26**(2005), 2, 223–232.

[15] Duda P., Mazurkiewicz G.: *Numerical modeling of heat and mass transfer in cylindrical ducts*. Arch. Thermodyn. 31(2010), 1, 33–43.

[16] Tandiroglu A.: *Effect of flow geometry parameters on transient heat transfer for turbulent flow in a circular tube with baffle inserts*. Int. J. Heat Mass Tran. **49**(2006), 9-10, 1559–1567.

[17] Nasiruddin, Kamran Siddiqui M.H.: *Heat transfer augmentation in a heat exchanger tube using a baffle*. Int. J. Heat Fluid Fl. **28**(2007), 2, 318–328.

[18] Zima W., Dziewa P.: *Mathematical modelling of heat transfer in liquid flat-plate solar collector tubes*. Arch. Thermodyn. **31**(2010), 2, 45–62.

[19] Kahalerras H., Targui N.: *Numerical analysis of heat transfer enhancement in a double pipe heat exchanger with porous fins*. Int. J. Numerical Meth. Heat and Fluid Flow **18**(2008), 5, 593–617.

[20] Sripattanapipat S., Promvonge P.: *Numerical analysis of laminar heat transfer in a channel with diamond-shaped baffles*. Int. Commun. Heat Mass **36**(2009), 1, 32–38.

[21] Rao Y., Xu Y., Wan C.: *An experimental and numerical study of flow and heat transfer in channels with pin fin-dimple and pin fin arrays*. Exp. Therm. Fluid Sci. **38**(2012), 237–247.

[22] Alam T., Saini R.P., Saini J.S.: *Experimental investigation on heat transfer enhancement due to V-shaped perforated blocks in a rectangular duct of solar air heater*. Energ. Convers. Manage. **81**(2014), 374–383.

[23] Kumar A., Kim M.H.: *Convective heat transfer enhancement in solar air channels*. Appl. Thermal Eng. 89(2015), 239–261.

[24] Kumar R., Sethi M., Chauhan R., Kumar A.: *Experimental study of enhancement of heat transfer and pressure drop in a solar air channel with discretized broken V-pattern baffle*. Renew. Energ. **101**(2017), 856–872.

[25] Wang F., Zhang J., Wang S.: *Investigation on flow and heat transfer characteristics in rectangular channel with drop-shaped pin fins*. Propulsion Power Res. **1**(2012), 1, 64–70.

[26] Chamoli S.: *A Taguchi approach for optimization of flow and geometrical parameters in a rectangular channel roughened with V down perforated baffles*. Case Stud. Therm. Eng. **5**(2015), 59–69.

[27] Du B.C., He Y.L., Wang K., Zhu H.H.: *Convective heat transfer of molten salt in the shell-and-tube heat exchanger with segmental baffles*. Int. J. Heat Mass Trans. **113**(2017), 456–465.

[28] Mohammadi Pirouz M., Farhadi M., Sedighi K., Nemati H., Fattahi E.: *Lattice Boltzmann simulation of conjugate heat transfer in a rectangular channel with wall-mounted obstacles*. Sci. Iran. B **18**(2011), 2 213–221.

[29] Jedsadaratanachai W., Boonloi A.: *Effects of blockage ratio and pitch ratio on thermal performance in a square channel with 30° double V-baffles*. Case Stud. Therm. Eng. **4**(2014), 118–128.

[30] Zhao H., Liu Z., Zhang C., Guan N., Zhao H.: *Pressure drop and friction factor of a rectangular channel with staggered mini pin fins of different shapes*. Exp. Therm. Fluid Sci. **71**(2016), 57–69.

[31] Tahmasebi A., Mahdavi M., Ghalambaz M.: *Local thermal nonequilibrium conjugate natural convection heat transfer of nanofluids in a cavity partially filled with porous media using Buongiorno's model*. Numer. Heat Tr. A-Appl. **73**(2018), 4, 254–276.

[32] Mehryan S.A.M., Ghalambaz M., Izadi M.: *Conjugate natural convection of nanofluids inside an enclosure filled by three layers of solid, porous medium and free nanofluid using Buongiorno's and local thermal non-equilibrium models*. J. Therm. Anal. Calorim. **135**(2019), 2, 1047–1067.

[33] Mehryan S.A.M., Izadpanahi E., Ghalambaz M., Chamkha A.J.: *Mixed convection flow caused by an oscillating cylinder in a square cavity filled with Cu-Al_2O_3/water hybrid nanofluid*. J. Therm. Anal. Calorim. **137**(2019), 965–982.

[34] Mehryan S.A.M., Kashkooli F.M., Ghalambaz M., Chamkha A.J.: *Free convection of hybrid Al_2O_3-Cu water nanofluid in a differentially heated porous cavity*. Adv. Powder Technol. **28**(2017), 9, 2295–2305.

[35] Ghalambaz M., Doostani A., Izadpanahi E., Chamkha A.J.: *Phase-change heat transfer in a cavity heated from below: The effect of utilizing single or hybrid nanoparticles as additives*. J. Taiwan Inst. Chem. Eng. **72**(2017), 104–115.

[36] Ghalambaz M., Doostani A., Chamkha A.J., Ismael M.A.: *Melting of Nanoparticles-Enhanced Phase-Change Materials in an Enclosure: Effect of Hybrid Nanoparticles*. Int. J. Mech. Sci. **134**(2017), 85–97.

[37] Ghalambaz M., Jamesahar E., Ismael M.A, Chamkha A.J.: *Fluid-structure interaction study of natural convection heat transfer over a flexible oscillating fin in a square cavity*. Int. J. Therm. Sci. **111**(2017), 256–273.

[38] Chamkha A.J., Doostanidezfuli A., Izadpanahi E., Ghalambaz M.: *Phase-change heat transfer of single/hybrid nanoparticles-enhanced phase-change materials over a heated horizontal cylinder confined in a square cavity*. Adv. Powder Technol. **28**(2017), 2, 385–397.

[39] Menni Y., Azzi A.: *Computational fluid dynamical analysis of turbulent heat transfer in a channel fitted with staggered V-Shaped baffles*. WJMS **14**(2018), 2, 108–123.

[40] Feng Z., Ivan C.: *Numerical evaluation of flow and heat transfer in plate-pin fin heat sinks with various pin cross-sections*. Numer. Heat Tr. A-Appl. **60**(2011), 2, 107–128.

[41] Dittus F.W., Boelter L.M.K.: *Heat transfer in automobile radiators of tubular type*. Int. Commun. Heat **12**(1985), 1, 3–22.

[42] Petukhov B.S.: *Heat transfer and friction in turbulent pipe flow with variable physical properties*. Adv. Heat Transf. **6**(1970), 503–564,

[43] Patankar S.V.: *Numerical heat transfer and fluid flow*. McGraw-Hill, New York 1980.

[44] Leonard B.P., Mokhtari S.: *ULTRA-SHARP nonoscillatory convection schemes for high-speed steady multidimensional flow*. NASA TM 1-2568, NASA Lewis Research Center, 1990.